Spin- and valley-polarized transport in a monolayer of MoS_2

P. M. Krstajić*
Center of Microelectronic Technologies and Single Crystals (IHTM), University of Belgrade, Njegoševa 12, 11000 Belgrade, Serbia

P. Vasilopoulos† and M. Tahir‡
Department of Physics, Concordia University, 7141 Sherbrooke Ouest, Montréal, Québec H4B 1R6, Canada
(Received 21 January 2016; revised manuscript received 21 June 2016; published 15 August 2016)

We investigate dc and ac transport in a monolayer of MoS_2 in the presence of an effective mass asymmetry, a momentum-dependent term, and an out-of plane or in-plane Zeeman term. Analytical results are presented for both dc and ac conductivities in the framework of linear response theory. We show that the spin-Hall conductivity exhibits a strong dependence on the strength of the spin-orbit interaction while both spin- and valley-Hall conductivities show a very weak dependence on the temperature. The sum of the well separated spin-up and spin-down components of the diffusive dc longitudinal conductivity is linear in the electron concentration though the Fermi level is a nonmonotonic function of it. Further, we evaluate the power absorption spectrum and assess its dependence on the spin and valley degrees of freedom as well as on the scattering which is essential at low frequencies.

DOI: 10.1103/PhysRevB.94.085413

I. INTRODUCTION

Two-dimensional (2D) materials are being explored extensively since the discovery of graphene and its potential applications in various fields [1]. Although graphene possesses extraordinary properties, its application in device fabrication is limited by its zero band gap and very weak spin-orbit interaction (SOI). For instance, graphene transistors suffer from a low on-off current ratio due to its gapless structure [2]. This led to intensive investigations of alternative materials with a finite band gap such as silicene [3], germanene [4], and group-VI transition-metal dichalcogenides (e.g., $MX_2, M =$ Mo,W; $X =$ S,Se) [5–9]. Recently it has been demonstrated that a monolayer of MoS_2, a typical transition-metal dichalcogenide, is a semiconductor with a relatively large direct band gap ($2\Delta' = 1.66$ eV) and a very strong SOI ($2\lambda = 150$ meV). The degenerate K and K′ valleys are related to each other by time-reversal symmetry and give rise to the valley degree of freedom of the band-edge electrons and holes [10–13]. A monolayer of MoS_2 has a reasonable in-plane carrier mobility, high thermal stability, and good compatibility with standard semiconductor technology [14]. These properties render MoS_2 a promising candidate for a wide range of applications, including photoluminescence at visible wavelengths [10,15], photodetectors with high responsivity [12], and field-effect transistors [14,16,17].

Further, dc [18–20] and ac [21–24] transport properties of MoS_2 have been of continuing strong interest and studied extensively. However, these studies are limited. The dc studies are based on the model Dirac-type Hamiltonian introduced in Ref. [7]. However, based on the tight-binding [25,26] and $\mathbf{k}\cdot\mathbf{p}$ methods [27], it has been shown that going beyond such a Hamiltonian by including an effective-mass asymmetry, and a quadratic momentum-dependent term, is very important as each of these terms can have serious physical consequences. For example, due to the SOI and the momentum quadratic term (α), the two-band model reveals a particle-hole asymmetry and a term β gives a contribution to the Chern number at each valley [22]. The ac studies [21–24] have not considered the Zeeman term which has been assessed in recent experiments [28–31] and theoretically shown to be approximately 30 meV by first-principles calculations [32]. The Zeeman exchange field ($M_z = g'\mu_B B/2$) can be induced by ferromagnetic order, g' the Landé g factor ($g' = g'_e + g'_s$), and μ_B the Bohr magneton [27]. Also, $g'_e = 2$ is the free-electron g factor, and $g'_s = 0.21$ is the out-of-plane factor due to the strong SOI in MoS_2. Accordingly, dc and ac transport studies are timely and expected to increase our understanding of this material's family. As will be shown, an important difference between previous studies and our work is the inclusion of an effective-mass asymmetry, a quadratic momentum-dependent term, and the Zeeman term. Another difference is that we take into account a more complete frequency response to external fields by including the scattering-dependent diffusive part, in the manner of Ref. [33] for silicene, that was previously neglected. This substantially affects the power absorption spectrum at low frequencies.

In this paper we study dc and ac quantum transport properties of a MoS_2 monolayer. We derive and discuss its band structure in the presence of an effective-mass asymmetry, a quadratic momentum-dependent term, as well as an out-of plane or in-plane Zeeman term. The evaluation is done with Kubo-type formulas expressed explicitly in terms of single-particle eigenstates and eigenvalues. We evaluate the dc and ac spin- and valley-Hall conductivities as well as the longitudinal conductivity. The formalism is presented in Sec. II, dc conductivity results in Sec. III, and the ac ones in Sec. IV. We also evaluate the power absorption spectrum in Sec. V and summarize in Sec. VI.

*predrag222@gmail.com
†p.vasilopoulos@concordia.ca
‡m.tahir06@alumni.imperial.ac.uk

II. FORMALISM

We consider a monolayer of MoS_2 in the (x,y) plane. Particles in MoS_2 are described by the 2D Dirac-type Hamiltonian

$$H_{s_z}^{\eta} = v(\eta\sigma_x p_x + \sigma_y p_y) + \Delta'\sigma_z + (I-\sigma_z)\eta s_z\lambda' + rk^2(\alpha I + \beta\sigma_z) + s_z M_z\,. \tag{1}$$

Here $r = \hbar^2/4m_0$, $\eta = \pm 1$ for valleys K and K′, $\Delta' = \Delta/2$, Δ is the mass term that breaks the inversion symmetry, $\lambda' = \lambda/2$, λ is the SOI strength, σ_i, $i = x,y,z$, are the Pauli matrices for the valence and conduction bands, and I is the identity matrix. The parameters α and β depend on the (unequal) electron and hole effective masses and thus pertain to the effective mass asymmetry [34]. Their values for MoS_2 are $\alpha = 0.43$ and $\beta = 2.21$, see Ref. [34]. Further, $s_z = 1(-1)$ is for spins up (down), M_z is the exchange field, and v denotes the Fermi velocity of the electrons. With $c_k = \hbar vk$, $\Delta_\xi = \Delta' - \lambda'\xi + \beta rk^2$, and $\xi = \eta s_z$, the eigenvalues pertaining to Eq. (1) are

$$E_{s,t}^{\eta} = \eta s_z\lambda' + s_z M_z + \alpha rk^2 + t\left[c_k^2 + \Delta_\xi^2\right]^{1/2}. \tag{2}$$

The corresponding eigenfunctions are written as

$$\Psi_{s,t}^{\eta} = \begin{pmatrix} \frac{\eta c_k e^{-i\eta\varphi}}{D_{\xi k}} \\ -\frac{\Delta_\xi - t\delta_{\xi k}}{D_{\xi k}} \end{pmatrix} e^{i\mathbf{k}\cdot\mathbf{r}}, \tag{3}$$

where

$$D_{\xi k} = \left[c_k^2 + (\Delta' + (\alpha+\beta)rk^2 - E_F - s_z M_z)^2\right]^{1/2} \tag{4}$$

with $t = +1$ for the conduction band and $t = -1$ for the valence band. The energy dispersion is shown in Fig. 1 for $\alpha = \beta = 0$ and (a) $M_z = 0$ and (b) $M_z = 50$ meV. Panels (c) and (d) correspond, respectively, to (a) and (b) but with $\alpha \neq 0$ and $\beta \neq 0$. The gap is $2\Delta'$, with $\Delta' = 830$ meV, the SOI strength $\lambda' = 37.5$ meV, $\alpha = 0.43$ and $\beta = 2.21$ (Ref. [34]). As can be seen, the terms proportional to α and β make a rather negligible contribution to the spectrum. This is essentially due to the large gap.

Equations (1)–(3) are valid for an out-of-plane Zeeman term. If we consider an in-plane Zeeman term, the Hamiltonian is given by Eq. (1) with its last term replaced by $\sigma_x M_x$. The corresponding eigenvalues are given by

$$E_{s,t}^{\eta} = \eta s_z\lambda' + \alpha rk^2 + t\left[c_k^2 + M_x^2 + 2M_x\eta\hbar vk_x + \Delta_\xi^2\right]^{1/2} \tag{5}$$

and the eigenfunctions by

$$\Psi_{s,t}^{\eta} = \begin{pmatrix} \frac{\eta c_k e^{-i\eta\varphi} + M_x}{D_{\xi k}} \\ -\frac{\Delta_\xi - t\delta_{\xi k}}{D_{\xi k}} \end{pmatrix} e^{i\mathbf{k}\cdot\mathbf{r}}, \tag{6}$$

The density of states corresponding to the spectrum (2) is $D(E) = \sum_\zeta \delta(E - E_\zeta)$ with $|\zeta\rangle = |t,\eta,s_z,k_x,k_y\rangle$. For $\alpha = \beta = 0$ and $M_x = 0$ it has the simple form

$$D(E) = \frac{1}{2\pi\hbar^2 v^2}\sum_{t\eta s_z} |E - \eta s_z\lambda' - s_z M_z|\Theta\big(|E - \eta s_z\lambda' - s_z M_z| - |\Delta_\xi^0|\big), \tag{7}$$

where $\Delta_\xi^0 = \Delta' - \eta s_z\lambda'$. For $\alpha \neq 0, \beta \neq 0$ though, $D(E)$ takes a more complicated form

$$D(E) = \frac{1}{2\pi}\sum_{t\eta s_z} \frac{|E - \eta s_z\lambda' - s_z M_z|\Theta\big(|E - \eta s_z\lambda' - s_z M_z| - |\Delta_\xi^0|\big)}{|2\alpha r|E - \eta s_z\lambda' - s_z M_z| + t(\hbar^2 v^2 + 2\beta r\Delta_\xi)|}\,. \tag{8}$$

We show $D(E)$ in Fig. 2 for (a) $M_z = 0$ meV and (b) $M_z = 50$ meV. The visible asymmetry between conduction and valence bands can also be deduced from Fig. 1. For instance, for $M_z = 0$ the conduction band starts at $E_c = \Delta'$ while the valence band is already split by the SOI at $k = 0$.

To evaluate the conductivities we follow the formalism presented in Ref. [35]. We consider a many-body system described by the Hamiltonian $H = H_0 + H_I - \mathbf{R}\cdot\mathbf{F}$, where H_0 is the unperturbed part, H_I is a binary type interaction, and $-\mathbf{R}\cdot\mathbf{F}$ is the interaction of the system with an external field $\mathbf{F}$ with $\mathbf{R} = \sum_i \mathbf{r}_i$ and $\mathbf{r}_i$ the position operator of electron i. In the case of interest $\mathbf{F} = e\mathbf{E}$, where $\mathbf{E}$ is the electric field and e the electron charge. In the representation in which H_0 is diagonal the many-body density operator ρ has a diagonal part ρ^d and nondiagonal part ρ^{nd}, $\rho = \rho^d + \rho^{nd}$. For weak electric fields and weak scattering the conductivity tensor has a diagonal and a nondiagonal part, $\sigma_{\mu\nu} = \sigma_{\mu\nu}^d + \sigma_{\mu\nu}^{nd}$, $\mu, \nu = x, y$.

In general there are two kinds of currents, diffusive and hopping, but usually only one of them is present. If there is no magnetic field the hopping contribution vanishes identically, see Eq. (2.65) in Ref. [35]. For elastic scattering the component $\sigma_{\mu\nu}^d$ is given by [35]

$$\sigma_{\mu\nu}^d = \frac{\beta e^2}{S}\sum_\zeta f_\zeta(1-f_\zeta)\,\frac{v_{\nu\zeta}\,v_{\mu\zeta}\,\tau_\zeta}{1 + i\omega\tau_\zeta}\,, \tag{9}$$

where ω is the frequency, τ_ζ the relaxation time, and $v_{\mu\zeta}$ the diagonal matrix element of the velocity operator $v_{\mu\zeta} = \langle\zeta|v_\mu|\zeta\rangle$ $(\mu = x, y)$ with $|\zeta\rangle = |t,\eta,s_z,k_x,k_y\rangle$ and S is the area of the system. Further, f_ζ is the Fermi-Dirac distribution $f_\zeta = [1 + \exp[\beta(E_\zeta - E_F)]]^{-1}$, $\beta = 1/k_B T$, and T the temperature.

As for the contribution $\sigma_{\mu\nu}^{nd}$, one can use the identity $f_{\zeta'}(1 - f_\zeta)[1 - e^{\beta(E_{\zeta'} - E_\zeta)}] = f_{\zeta'} - f_\zeta$ and cast the original expression [35] in the familiar form

$$\sigma_{\mu\nu}^{nd}(i\omega) = \frac{i\hbar e^2}{S}\lim_{\eta\to 0+}\sum_{\zeta\neq\zeta'}\frac{(f_\zeta - f_{\zeta'})\,v_{\nu\zeta\zeta'}\,v_{\mu\zeta'\zeta}}{(E_\zeta - E_{\zeta'})(E_\zeta - E_{\zeta'} + \hbar\omega - i\eta)}, \tag{10}$$

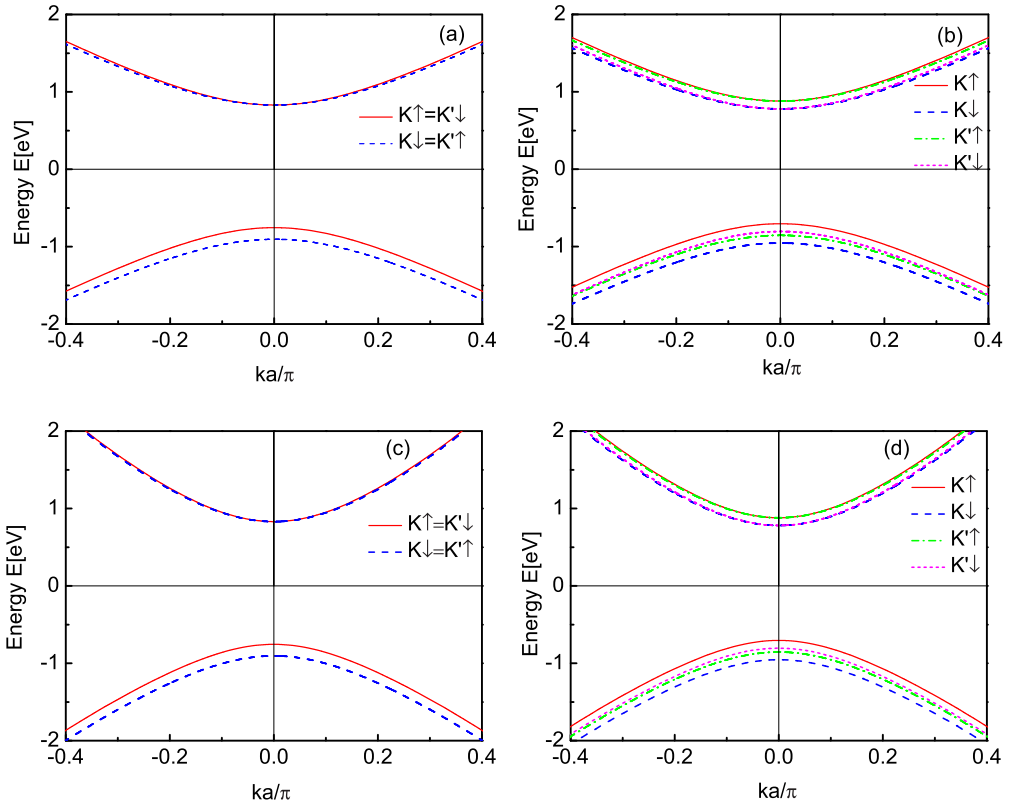

FIG. 1. Energy dispersion for (a) $M_z = 0$ and (b) $M_z = 50$ meV, both with $\alpha = \beta = 0$. (c) and (d): as in (a) and (b), respectively, with both with $\alpha \neq \beta \neq 0$. The parameters are $\Delta' = 830$ meV and $\lambda' = 37.5$ meV.

where $v_{\nu\zeta\zeta'} = \langle\zeta|v_\nu|\zeta'\rangle$ and $v_{\mu\zeta'\zeta} = \langle\zeta'|v_\mu|\zeta\rangle$ are the matrix elements of the velocity operators with $\nu, \mu = x, y$. The sum runs over all quantum states $|\zeta\rangle$ and $|\zeta'\rangle$ provided that $|\zeta\rangle \neq |\zeta'\rangle$. From now on, the infinitesimal quantity η in Eq. (10) will be replaced by Γ_ζ in order to account for the finite broadening of the energy levels.

III. DC TRANSPORT

The velocity operators $\hat{v}_x = \partial H/\partial(\hbar k_x)$ and $\hat{v}_y = \partial H/\partial(\hbar k_y)$ are obtained as $\hat{v}_x = \eta v \sigma_x$, $\hat{v}_y = v\sigma_y$. The product of their matrix elements $v_{x\zeta\zeta'} v_{y\zeta'\zeta}$ between electron and hole states that does not contain the factor $e^{-i\eta\varphi}$, indicated below by the subscript 0, is equal to

$$(v_{x\zeta\zeta'} v_{y\zeta'\zeta})_0 = i\eta v^2 c_k^2 \, \frac{4\Delta_\xi \delta_{\xi k}}{D_{\xi k}^2 D_{\xi k}'^2} \, \delta_{\mathbf{k},\mathbf{k}'} \delta_{s_z,s_z'} \delta_{\eta,\eta'} \,, \tag{11}$$

where $D_{\xi k}$ and $D'_{\xi k}$ are the normalization factors for the valence and conduction bands, cf. Eq. (4). It can easily be proven

$$(v_{x\zeta\zeta'} v_{y\zeta'\zeta})_0 = (i\eta v^2 \Delta_\xi / \delta_{\xi k}) \, \delta_{\mathbf{k},\mathbf{k}'} \delta_{s_z,s_z'} \delta_{\eta,\eta'} \,. \tag{12}$$

The product of the velocity matrix elements between hole and electron states has the opposite sign, i.e., $(v_{x\zeta'\zeta} v_{y\zeta\zeta'})_0 = -(v_{x\zeta\zeta'} v_{y\zeta'\zeta})_0$. Notice that terms containing the phase factor

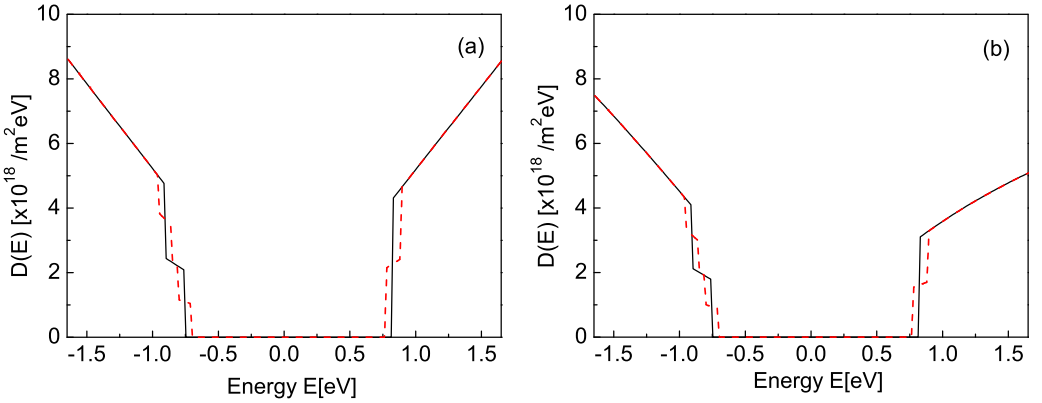

FIG. 2. Density of states in MoS_2 for (a) $\alpha = \beta = 0$ and (b) $\alpha \neq 0$ and $\beta \neq 0$. The black, solid curve is for $M_z = 0$ meV and the red, dashed one for $M_z = 50$ meV.

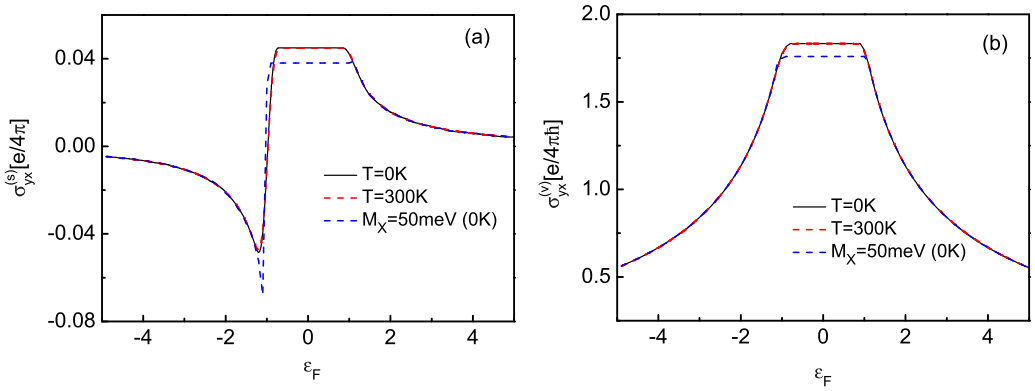

FIG. 3. (a) Spin-Hall conductivity vs Fermi energy for temperatures $T = 0$ K and $T = 300$ K, $M_z = 50$ meV and $M_x = 0$ meV. The red and black curves are for an out-of plane Zeeman term and the blue dashed one for an in-plane Zeeman term with $T = 0$ K, $M_x = 50$ meV, and $M_z = 0$ meV. (b) As in (a) for the valley-Hall conductivity.

$e^{-i\eta\varphi}$ will yield zero contribution to the result because the energy spectrum is isotropic.

For an in-plane Zeeman term Eq. (11) takes the form

$$(v_{x\zeta\zeta'}v_{y\zeta'\zeta})_0 = i\eta v^2 \frac{4\left(c_k^2 - M_x^2\right)\delta_{\xi k}\Delta_\xi}{D_{\xi k}^2 D_{\xi k}'^2}\,\delta_{\mathbf{k},\mathbf{k}'}\delta_{s_z,s_z'}\delta_{\eta,\eta'}\,. \quad (13)$$

First we neglect the broadening of the levels by setting $\Gamma_\zeta = 0$. Then Eq. (10) takes the form

$$\sigma_{yx}^{nd}(\eta,s_z) = \frac{\eta\hbar e^2 v^2}{2S}\sum_{\mathbf{k}}(f_{-,\mathbf{k}} - f_{+,\mathbf{k}})\left(\Delta_\xi/\delta_{\xi k}^3\right). \quad (14)$$

From Eq. (14) we determine the spin-Hall and valley-Hall conductivities, respectively, as

$$\sigma_{yx}^{(s)} = \sum_\eta \left[\sigma_{yx}^{nd}(\eta,s_z=+1) - \sigma_{yx}^{nd}(\eta,s_z=-1)\right], \quad (15)$$

and

$$\sigma_{yx}^{(v)} = \sum_{s_z} \left[\sigma_{yx}^{nd}(\eta=+1,s_z) - \sigma_{yx}^{nd}(\eta=-1,s_z)\right]. \quad (16)$$

Note that the charge conductivity $\sigma_{yx}^{(\text{charge})} = \sum_{\eta,s_z}\sigma_{yx}^{nd}(\eta,s_z)$ is equal to zero.

In Figs. 3(a) and 3(b) we plot the spin- and valley-Hall conductivities vs normalized Fermi level $\varepsilon_F = E_F/\Delta'$. The black and red curves correspond to an out-of-plane exchange field $M_z = 50$ meV ($M_x = 0$ meV), while the dashed, blue one to an in-plane field $M_x = 50$ meV ($M_z = 0$ meV). The spin-Hall conductivity is rather nonmonotonic in the vicinity of the valence band while in the valley-Hall conductivity this behavior is smeared out by summation over spin, see Eq. (16). The flat regions in the graphs near $\varepsilon_F = 0$ are due to the fact that factor $f_{-,\mathbf{k}} - f_{+,\mathbf{k}}$ is constant when ε_F lies in the gap. The slight reduction in their gap values is due to the different numerators in Eqs. (11) and (13). If we use $M_z = 0$ meV or $M_x = 0$ meV, the results, not shown, are near identical with those shown because M_z and M_x are much smaller than the band gap $2\Delta'$.

In Fig. 4(a) we present the spin-Hall conductivity and in Fig. 4(b) the valley-Hall conductivity vs an *out-of-plane* exchange field M_z, with $M_x = 0$, for $E_F(= -1$ eV) inside the valence band and two different temperatures $T = 0$ K (solid black curve) and $T = 300$ K (red dashed curve). A kink in both graphs occurs, when E_F crosses the spin-down branch of the K valley, at $M_{zcr} = -(E_F + 2\lambda' + \Delta) = 95$ meV. The difference between the results of the two temperatures appears larger than in Fig. 3 due to the different scale used. In Fig. 5 we show the spin-Hall and valley-Hall conductivities versus an *in-plane* exchange field M_x with $M_z = 0$. In both panels we have $E_F = -1$ eV. Although the conductivity values are comparable to those for an *out-plane* exchange field shown in Fig. 4, we also see two qualitative differences: In Fig. 5(a) we don't see any increase as in Fig. 4(a) and in Fig. 5(b) no peak

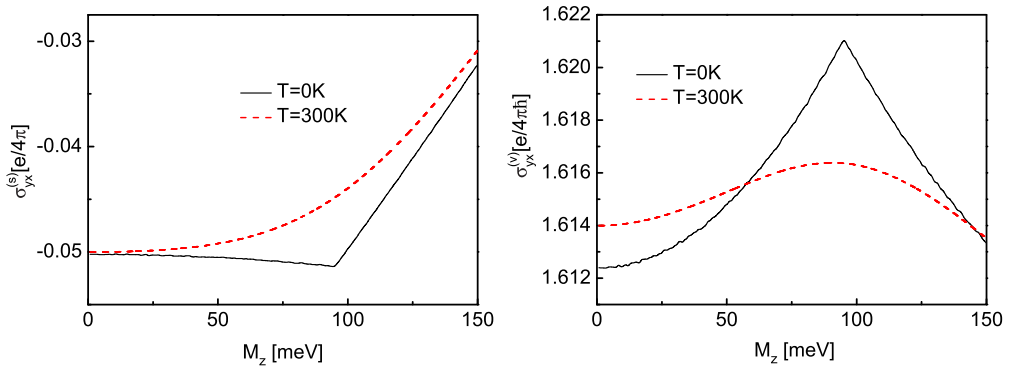

FIG. 4. (a) Spin-Hall conductivity vs field M_z for two different temperatures $T = 0$ K and $T = 300$ K. (b) As in (a) for the valley-Hall conductivity. In both panels $E_F = -1$ eV.

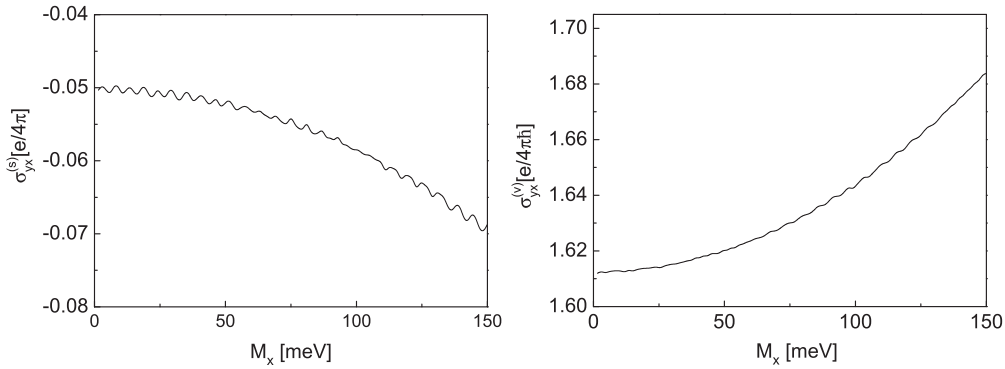

FIG. 5. (a) Spin-Hall conductivity vs field M_x. (b) As in (a) for the valley-Hall conductivity. In both panels $E_F = -1$ eV.

as in Fig. 4(b). The weak oscillations present in Figs. 5(a) and 5(b) are due to the presence of M_x in the eigenvector Eq. (6), as well as the term $M_x k_x$ in the eigenvalues, Eq. (5).

Further, we varied the SOI parameter λ', for $E_F = -1$ eV, and show the spin-Hall conductivity, in Fig. 6(a), and the valley-Hall conductivity in Fig. 6(b), both versus λ'. The solid black and red dashed curves are for $M_z = 50$ meV, the blue dotted one for $M_z = 0$ meV and $T = 0$ K. As in Figs. 3 and 4, the calculations are done for two different temperatures: $T = 0$ K (solid black and blue dotted curves) and $T = 300$ K (red dashed curve). The cusps visible in both panels occur when E_F crosses the spin and valley subbands. As expected, for $M_z = 0$ meV (blue dotted curve) there are fewer cusps.

Next we proceed with the evaluation of the longitudinal conductivity σ_{xx}^d. It is given by the $\omega \to 0$ limit of Eq. (21), valid for very low temperatures, and reads

$$\sigma_{xx}^d(\eta, s_z) = \frac{e^2\hbar^2 v^4}{4\pi} \sum_{t=\pm 1} \int_0^\infty \left(k^3 \tau_{tk} / \delta_{\xi k}^2\right) \delta(E_{tk} - E_F)\, dk\,. \tag{17}$$

Evaluating τ_{tk} at the Fermi level $E_F' = E_F - \eta s_z \lambda' - s_z M_z$ and integrating over k gives

$$\sigma_{xx}^d(\eta, s_z) = \frac{e^2 v^4}{4\pi} \frac{k_F^2 \tau_F}{S_F \delta_{\xi k_F}} \Theta(|E_F'| - |\Delta_\xi|)\,, \tag{18}$$

with S_F given in Eq. (23).

In Fig. 7 we show the longitudinal conductivity σ_{xx}^d, for (a) the K valley, and (b) the K′ valley as a function of the electron concentration n_c for $M_z = 50$ meV and $M_x = 0$. The red dotted curve is for spins up, the blue dashed one for spins down, and the dash-dotted black curve is the sum of the two valley contributions. We emphasize that the black solid curve is the sum of the red dotted (spin-up) and the blue dashed (spin-down) lines. In Fig. 7(a) the red dotted and the black solid curves coincide because the spin-up component (blue, solid line) for the K valley is zero. The dependence of the total σ_{xx}^d (dash-dotted curve) on n_c is monotonic and linear despite the fact E_F and the density of states are not. It can be seen that the spin-up and spin-down components have threshold values when E_F crosses the spin subbands.

IV. AC TRANSPORT

In this section we evaluate spin- and valley-Hall conductivities for finite frequency, level broadening, and temperature. We assume that the level broadening Γ_ζ is the same for all levels $\Gamma_\zeta \approx \Gamma$. Using the original formula for σ_{yx}^{nd}, Eqs. (2)–(4), and Eq. (10) we obtain

$$\sigma_{yx}^{nd}(i\omega, \eta, s_z) = \frac{\eta\hbar e^2 v^2}{2S} \sum_{\mathbf{k}, n=\pm 1} \frac{(f_{-,\mathbf{k}} - f_{+,\mathbf{k}})\Delta_\xi}{\delta_{\xi k}^2} \times \frac{2\delta_{\xi k} + n\alpha_0\Delta' + ni\Gamma}{(2\delta_{\xi k} + n\alpha_0\Delta')^2 + \Gamma^2}\,, \tag{19}$$

where $\alpha_0 = \hbar\omega/\Delta'$. In Fig. 8(a) we show the spin-Hall conductivity and in Fig. 8(b) the valley-Hall one vs the dimensionless parameter α_0. The solid curves are for $\alpha, \beta \neq 0$

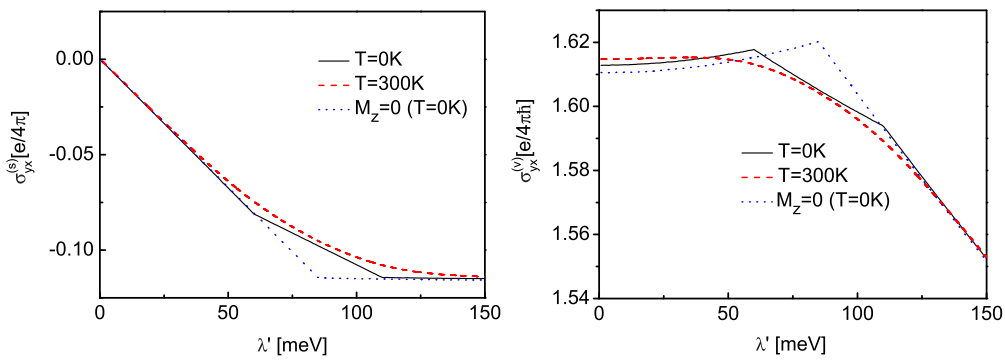

FIG. 6. (a) Spin-Hall conductivity vs SOI parameter λ' for two temperatures, $T = 0$ K and $T = 300$ K. (b) As in (a) for the valley-Hall conductivity. In either panel $E_F = -1$ eV and the blue dotted curve is for $M_z = 0$ meV and $T = 0$ K.

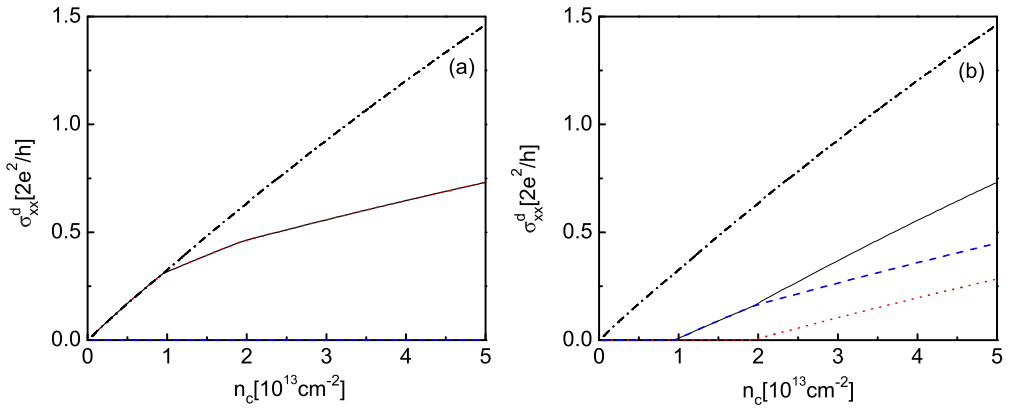

FIG. 7. Longitudinal conductivity σ^d_{xx} (black solid line) in units of $2e^2/h$ for (a) the K valley and (b) the K′ valley, and their spin-up (red dotted curve) and spin-down (blue dashed curve) components vs electron concentration n_c. The black dash-dotted curve in both panels is the total σ^d_{xx}. Here $M_z = 50$ meV and $M_x = 0$.

($\Gamma = 20$ meV), the red dotted ones for $\alpha = \beta = 0$ ($\Gamma = 20$ meV), while the green dashed curves correspond to the same $\alpha, \beta \neq 0$ but smaller broadening ($\Gamma = 5$ meV). $E_F(=0)$ is taken in the middle of the gap and $M_z = 50$ meV. The blue dash-dotted curve corresponds to an *in-plane* exchange field M_x. The double kink in the valley-Hall conductivity is due to the small but finite Γ; it is smeared out for larger Γ, (compare the solid and green dashed curves). The difference between the solid and dotted curves is due to the effective mass asymmetry and quadratic momentum-dependent term and highlights the importance of this term. The abrupt change of the spin-Hall conductivity in Fig. 8(a) for $\alpha_0 \approx 2$ is due to the presence of the term $2\delta_{\xi k} - \alpha_0\Delta'$ (for $n = -1$) in Eq. (19) since $\delta_{\xi k} \approx \Delta'$ ($\Delta' \gg \lambda'$). Furthermore, the peak at $\alpha_0 \approx 2$ indicates significant interband transitions since the gap is equal to $2\Delta'$. Similar to Figs. 3(a) and 3(b), if we use an exchange field $M_z = 0$ meV or $M_x = 0$ meV, the results change very little again because M_z and M_x are much smaller than the band gap $2\Delta'$. These results agree with those of Ref. [21]. For $\alpha = \beta = 0$ the $\omega \to 0$ and $T \to 0$ limit of Eq. (19), with $M_x = 0$ meV and the Fermi level inside the band gap, is real and reads

$$\sigma^{nd}_{yx}(\eta, s_z) = \frac{e^2}{h}\frac{\eta\Delta_\xi}{\Gamma}\arccos\left(|\Delta_\xi|/\left[\Delta_\xi^2 + \Gamma^2/4\right]^{1/2}\right). \quad (20)$$

With $\Gamma \to 0$ and de l' Hôpital's rule Eq. (20) turns into $\sigma^{nd}_{yx}(\eta, s_z) = (\eta e^2/2h)\cdot \mathrm{sgn}(\Delta_\xi)$. This is similar to the dc result of Ref. [33] for silicene which involves a very different Δ_ξ.

Next we proceed with the evaluation of the ac longitudinal conductivity for $M_z \neq 0$ and $M_x = 0$. Using the approximation $\beta f_\zeta(1 - f_\zeta) = -\partial f_\zeta/\partial E_\zeta \approx \delta(E_\zeta - E_F)$ for very low temperatures, $v_{x\zeta} = \hbar v k/2\delta_{\xi k}$, and starting from Eq. (9) one arrives at

$$\sigma^d_{xx}(i\omega, \eta, s_z) = \frac{e^2\hbar^2 v^4}{4\pi}\sum_{t=\pm1}\int_0^\infty \frac{k^3}{\delta^2_{\xi k}}\frac{\tau_{tk}}{1 + i\omega\tau_{tk}} \times \delta(E_{tk} - E_F)\, dk\,. \quad (21)$$

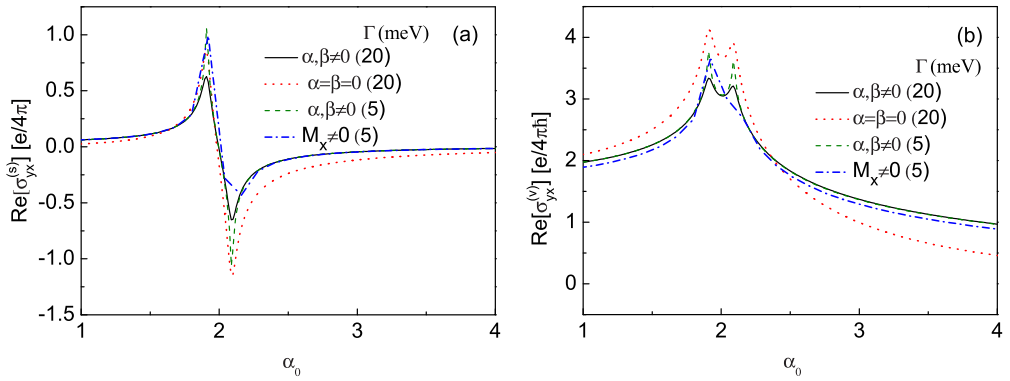

FIG. 8. (a) Spin-Hall conductivity vs frequency at $T = 0$ K. (b) As in (a) for the valley-Hall conductivity. The solid curves are for $\alpha, \beta \neq 0$ ($\Gamma = 20$ meV), the red dotted ones for $\alpha = \beta = 0$ ($\Gamma = 20$ meV), and the green dashed curves for the same $\alpha, \beta \neq 0$ but a smaller $\Gamma = 5$ meV. The blue dash-dotted curve is for an in-plane exchange field $M_x = 50$ meV, with $M_z = 0$, the other curves are for an out-of-plane exchange field $M_z = 50$ meV, with $M_x = 0$. In both panels $E_F = 0$.

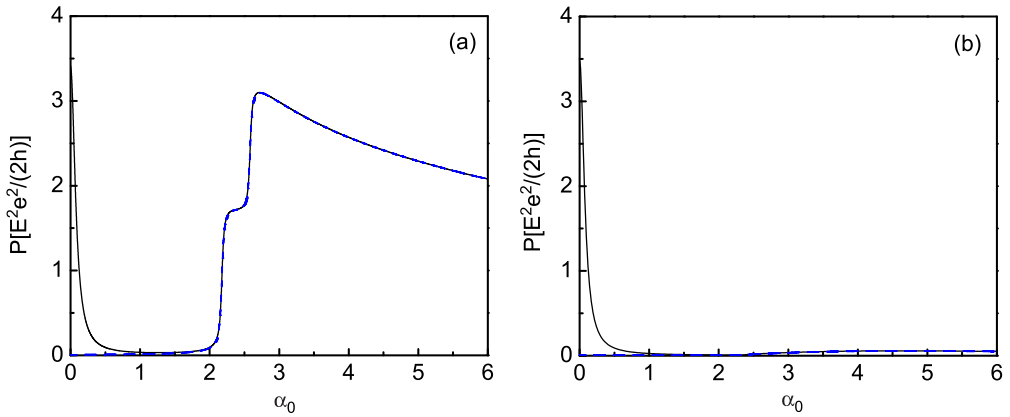

FIG. 9. Power spectrum vs $\alpha_0 = \hbar\omega/\Delta'$ in units of $E^2e^2/2h$ for (a) the K valley and (b) the K′ valley. The blue dashed curve is without contribution from σ^d_{xx}. In either case we used $\tau_F = 10^{-14}$ s, $M_z = 50$ meV, $M_x = 0$, and $E_F = 1$ eV.

Performing the integration in Eq. (21) and setting $\tau_{tk} \approx \tau_F$ one gets the final result for σ^d_{xx}

$$\sigma^d_{xx}(i\omega,\eta,s_z) = \frac{e^2v^4}{4\pi}\frac{k_F^2}{S_F\,\delta_{\xi k_F}}\frac{\tau_F}{1+i\omega\tau_F}\,\Theta(|E'_F|-|\Delta_\xi|)\,, \tag{22}$$

where

$$S_F = v^2 + \big(\alpha\delta_{\xi k_F} + \beta\Delta_\xi\big)/2m_0\,,$$
$$k_F^2 = (-B+\sqrt{B^2-4AC}\,)/2A\,, \tag{23}$$

with $A = r^2(\alpha^2-\beta^2)$, $B = -2r[\alpha E'_F + \beta(\Delta' - \eta s_z\lambda')] - \hbar^2v^2$, and $C = E'^2_F - (\Delta' - \eta s_z\lambda')^2$.

As far as the nondiagonal part σ^{nd}_{xx} of σ_{xx} is concerned, we first evaluate the product of matrix elements of velocity operators,

$$(v_{x\zeta\zeta'}v_{x\zeta'\zeta})_0 = v^2\big(\Delta_\xi^2+\delta_{\xi k}^2\big)/2\delta_{\xi k}^2. \tag{24}$$

Now taking into account Eq. (10) and Eq. (24) we arrive at

$$\sigma^{nd}_{xx}(i\omega,\eta,s_z) = \frac{i\hbar e^2v^2}{4S}\sum_{\mathbf{k},n=\pm1}\mathrm{sgn}(n)\,(f_{+,\mathbf{k}}-f_{-,\mathbf{k}}) \times\frac{\Delta_\xi^2+\delta_{\xi k}^2}{\delta_{\xi k}^3}\,\frac{2\delta_{\xi k}+n\alpha_0\Delta'+ni\Gamma}{(2\delta_{\xi k}+n\alpha_0\Delta')^2+\Gamma^2}\,. \tag{25}$$

We note that for circularly polarized light its handedness is expressed by the combination [7,21,36] $\sigma^{\pm}(\omega) = \sigma_{xx}(\omega) \pm i\sigma_{xy}(\omega)$, with σ^+ (σ^-) for right (left) polarization.

V. POWER SPECTRUM

Within linear response theory the average power absorbed from circularly polarized light of frequency ω and electric field E is given by

$$P(\omega,\eta,s_z) = (E^2/2)\mathrm{Re}\{\sigma_{xx}(i\omega,\eta,s_z)+\sigma_{yy}(i\omega,\eta,s_z) - i\sigma_{xy}(i\omega,\eta,s_z)+i\sigma_{yx}(i\omega,\eta,s_z)\}. \tag{26}$$

We remark that $\sigma_{xx}(i\omega,\eta,s_z) = \sigma_{yy}(i\omega,\eta,s_z)$ and $\sigma^{nd}_{xy}(i\omega,\eta,s_z) = -\sigma^{nd}_{yx}(i\omega,\eta,s_z)$. Further, we have $\sigma^d_{yx}(i\omega,\eta,s_z) = -\sigma^d_{xy}(i\omega,\eta,s_z) = 0$, see Ref. [35]. Then Eq. (26) simplifies to

$$P(\omega,\eta,s_z) = E^2\mathrm{Re}\big\{\sigma^d_{xx}(i\omega,\eta,s_z)+\sigma^{nd}_{xx}(i\omega,\eta,s_z) + i\sigma^{nd}_{yx}(i\omega,\eta,s_z)\big\}. \tag{27}$$

We consider the two valleys separately but sum over both spin directions. Thus, with $L = K, K'$, we write

$$P(\omega,L) = P(\omega,L,1)+P(\omega,L,-1). \tag{28}$$

In Fig. 9 we present the power spectrum versus the dimensionless parameter $\alpha_0 = \hbar\omega/\Delta'$ in units of $E^2e^2/2h$ for (a) the K valley (b) the K′ with $M_z = 50$ meV and $M_x = 0$ in both panels. We assumed a relaxation time $\tau_F = 10^{-14}$ s and $E_F = 1$ eV placed inside the conduction band. The initial high values are due to the contribution of the longitudinal conductivity σ^d_{xx} which in the limit $\omega \to 0$ gives, as it should, a Drude-type result, see Eq. (18) for $T \to 0$. This is evident by contrasting, in both panels, the black solid curve, which contains the scattering-dependent contribution from σ^d_{xx}, with the blue dashed curve which does not. As shown, this contribution is very important for low frequencies and would be missed if scattering was neglected. Furthermore, the visible jump occurs at $\alpha_0 \approx 2$ due to the term $(2\delta_{\xi k} - \hbar\omega)^2$

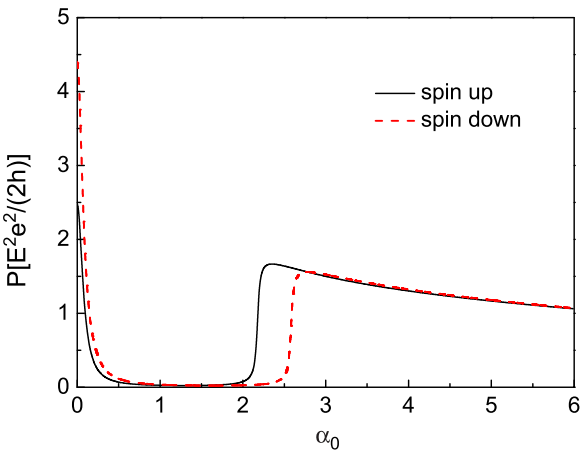

FIG. 10. Power spectrum vs $\alpha_0 = \hbar\omega/\Delta'$ in units of $E^2e^2/2h$ with $M_z = 50$ meV. The solid curve is for spins up, the dashed one for spins down, and $E_F = 1$ eV.

($\delta_{\xi k} \approx \Delta'$ for small k), that appears in the denominators of both Eqs. (19) and (25).

Finally, in Fig. 10 we show the spin dependence of the power spectrum by plotting the sum of the two valley contributions versus $\alpha_0 = \hbar\omega/\Delta'$ using the parameters of Fig. 9.

$$P(\omega, s_z) = P(\omega, K, s_z) + P(\omega, K', s_z). \tag{29}$$

The solid curve is for spins up and the dashed one for spins down. As seen, the up and down contributions are similar except for very low frequencies.

VI. SUMMARY

We derived analytical expressions for both dc and ac conductivities in a monolayer of MoS_2 using the framework of linear response theory. We showed that the spin-Hall conductivity depends strongly on the SOI strength while both spin- and valley-Hall conductivities show a very weak dependence on the temperature. The values of the valley-Hall conductivity are significantly larger that those of the spin-Hall one and both have nearly constant values when the Fermi energy lies in the gap. The diffusive longitudinal conductivity is linear in the electron concentration despite the fact that the Fermi level is a nonlinear function of this concentration. We also considered an *in-plane* Zeeman term M_x. The results are similar to those obtained with an *out-of-plane* Zeeman term M_z but substantial differences show up when the conductivities are plotted versus M_z or M_x, cf. Figs. 4 and 5. Finally, the power spectrum $P(\omega)$ for the K valley shows a rather high value for $\alpha_0 \to 0$ (or $\omega \to 0$) and a double jump at $\alpha_0 \approx 2$, due to the spin-up and spin-down responses occurring at different frequencies ω, cf. Fig. 10. Since the contribution to it from $\sigma^{nd}_{\mu\nu}$ almost vanishes in the interval $0 \leqslant \alpha_0 \approx 2$, cf. Fig. 8, the high value of $P(\omega)$ for $\omega \to 0$ is entirely due to the scattering-dependent components $\sigma^{d}_{\mu\mu}, \mu = x, y$ and would be missed if scattering was neglected. On the other hand, the power spectrum for the K′ valley decays monotonically with α_0.

ACKNOWLEDGMENTS

This work was supported by the Serbian Ministry of Education and Science, within the Project No. TR 32008 (PK) and the Canadian NSERC Grant No. OGP0121756 (PV, MT).

[1] A. H. Castro Neto, F. Guinea, N. M. R. Peres, K. S. Novoselov, and A. K. Geim, Rev. Mod. Phys. **81**, 109 (2009).
[2] L. Liao, Y.-C. Lin, M. Bao, R. Cheng, J. Bai, Y. Liu, Y. Qu, K. L. Wang, Y. Huang, and X. Duan, Nature (London) **467**, 305 (2010); F. Schwierz, Nat. Nanotechnol. **5**, 487 (2010).
[3] A. Kara, H. Enriquez, A. P. Seitsonen, L. C. Lew Yan Voon, S. Vizzini, B. Aufray, and H. Oughaddoub, Surf. Sci. **67**, 1 (2012); J. Sone, T. Yamagami, Y. Aoki, K. Nakatsuji, and H. Hirayama, New J. Phys. **16**, 095004 (2014).
[4] M. E. Dávila, L. Xian, S. Cahangirov, A. Rubio, and G. Le. Lay, New J. Phys. **16**, 095002 (2014).
[5] A. K. Geim and I. V. Grigorieva, Nature (London) **499**, 419 (2013).
[6] H. Fang, S. Chuang, T. C. Chang, K. Takei, T. Takahashi, and A. Javey, Nano Lett. **12**, 3788 (2012); H. Wang, L. Yu, Y.-H. Lee, Y. Shi, A. Hsu, M. L. Chin, L.-J. Li, M. Dubey, J. Kong, and T. Palacios, *ibid.* **12**, 4674 (2012); M. S. Fuhrer and J. Hone, Nat. Nanotechnol. **8**, 146 (2013).
[7] D. Xiao, G.-B. Liu, W. Feng, X. Xu, and W. Yao, Phys. Rev. Lett. **108**, 196802 (2012).
[8] H.-Z. Lu, W. Yao, D. Xiao, and S.-Q. Shen, Phys. Rev. Lett. **110**, 016806 (2013).
[9] X. Li, F. Zhang, and Q. Niu, Phys. Rev. Lett. **110**, 066803 (2013).
[10] A. Splendiani, L. Sun, Y. Zhang, T. Li, J. Kim, C.-Y. Chim, G. Galli, and F. Wang, Nano Lett. **10**, 1271 (2010).
[11] J. K. Ellis, M. J. Lucero, and G. E. Scuseria, Appl. Phys. Lett. **99**, 261908 (2011).
[12] H. S. Lee, S.-W. Min, Y.-G. Chang, M. K. Park, T. Nam, H. Kim, J. H. Kim, S. Ryu, and S. Im, Nano Lett. **12**, 3695 (2012).
[13] E. Cappelluti, R. Roldán, J. A. Silva-Guillén, P. Ordej ón, and F. Guinea, Phys. Rev. B **88**, 075409 (2013).
[14] B. Radisavljevic, A. Radenovic, J. Brivio, V. Giacometti, and A. Kis, Nat. Nanotechnol. **6**, 147 (2011).
[15] Q. H. Wang, K. Kalantar-Zadeh, A. Kis, J. N. Coleman, and M. S. Strano, Nat. Nanotechnol. **7**, 699 (2012).
[16] H. Liu, A. T. Neal, and P. D. Ye, ACS Nano **6**, 8563 (2012).
[17] Y. Yoon, K. Ganapathi, and S. Salahudin, Nano Lett. **11**, 3768 (2011).
[18] W. Feng, Y. Yao, W. Zhu, J. Zhou, W. Yao, and D. Xiao, Phys. Rev. B **86**, 165108 (2012).
[19] M. A. Cazalilla, H. Ochoa, and F. Guinea, Phys. Rev. Lett. **113**, 077201 (2014); M. Tahir, A. Manchon, and U. Schwingenschlogl, Phys. Rev. B **90**, 125438 (2014).
[20] Y. Ma, L. Kou, X. Li, Y. Dai, S. C. Smith, and T. Heine, Phys. Rev. B **92**, 085427 (2015).
[21] Z. Li and J. P. Carbotte, Phys. Rev. B **86**, 205425 (2012); C. J. Tabert and E. J. Nicol, *ibid.* **87**, 235426 (2013).
[22] H. Rostami and R. Asgari, Phys. Rev. B **89**, 115413 (2014).
[23] M. Gibertini, F. M. D. Pellegrino, N. Marzari, and M. Polini, Phys. Rev. B **90**, 245411 (2014).
[24] R. A. Muniz and J. E. Sipe, Phys. Rev. B **91**, 085404 (2015).
[25] H. Rostami, A. G. Moghaddam, and R. Asgari, Phys. Rev. B **88**, 085440 (2013).
[26] G.-B. Liu, W.-Y. Shan, Y. Yao, W. Yao, and D. Xiao, Phys. Rev. B **88**, 085433 (2013).
[27] A. Kormányos, V. Zólyomi, N. D. Drummond, and G. Burkard, Phys. Rev. X **4**, 011034 (2014).
[28] D. MacNeill, C. Heikes, K. F. Mak, Z. Anderson, A. Kormanyos, V. Zolyomi, J. Park, and D. C. Ralph, Phys. Rev. Lett. **114**, 037401 (2015).
[29] A. Srivastava, M. Sidler, A. V. Allain, D. S. Lembke, A. Kis, and A. Imamoglu, Nat. Phys. **11**, 141 (2015).
[30] G. Aivazian, Z. Gong, A. M. Jones, R.-L. Chu, J. Yan, D. G. Mandrus, C. Zhang, D. Cobden, W. Yao, and X. Xu, Nat. Phys. **11**, 148 (2015).
[31] Y. Li, J. Ludwig, T. Low, A. Chernikov, X. Cui, G. Arefe, Y. D. Kim, A. M. van der Zande, A. Rigosi, H. M. Hill, S. H. Kim,

J. Hone, Z. Li, D. Smirnov, and T. F. Heinz, Phys. Rev. Lett. **113**, 266804 (2014).

[32] Y. C. Cheng, Q. Y. Zhang, and U. Schwingenschlögl, Phys. Rev. B **89**, 155429 (2014).

[33] V. Vargiamidis, P. Vasilopoulos, and G-Q. Hai, J. Phys.: Condens. Matter **26**, 345303 (2014).

[34] L. Majidi, M. Zare, and R. Asgari, Solid State Commun. **199**, 52 (2014).

[35] M. Charbonneau, K. M. Van Vliet, and P. Vasilopoulos, J. Math. Phys. **23**, 318 (1982).

[36] M. Tahir, P. Vasilopoulos, and F. M. Peeters, Phys. Rev. B **93**, 035406 (2016).